

***In situ* observation of reversible deformation of Al foils during irradiation with MeV-energy ions**H. Tsuchida,^{1,*} I. Katayama,² S. C. Jeong,² M. Haba,¹ H. Ogawa,¹ N. Sakamoto,¹ H. Mori,³ J. G. Lee,³ and A. Itoh⁴¹*Department of Physics, Nara Women's University, Nara 630-8506, Japan*²*Institute of Particle and Nuclear Studies, KEK, Tsukuba 308-0801, Japan*³*Research Center for Ultra-High Voltage Electron Microscopy, Osaka University, Suita, Osaka 565-0871, Japan*⁴*Quantum Science and Engineering Center, Kyoto University, Kyoto 606-8501, Japan*

(Received 12 December 2003; published 31 August 2004)

Ion-irradiation-induced reversible deformation of Al foils has been studied using various MeV energy projectile ions of H^+ , C^{2+} , C^{3+} , O^{2+} , O^{3+} , Si^{3+} , and Si^{4+} . To find the source causing this foil-deformation, we performed systematic investigations from various aspects. It was found that the electronic energy deposition is the dominant driving force of deformation, and the deformation occurs at temperatures much below the recrystallization temperature of 200°C. Experimental results were analyzed in terms of conventional thermal models. It is concluded that the reversible deformation may be due to dynamical changes of thermophysical properties of materials during ion irradiation.

DOI: 10.1103/PhysRevB.70.054112

PACS number(s): 61.80.Jh, 62.20.Dc, 64.60.Ht

I. INTRODUCTION

In the past few years energetic fast ions have been extensively utilized as indispensable powerful tools in a wide range of nanotechnology-based materials science covering element analysis, fine processing and structural modification of materials.^{1,2} On the other hand, ion-irradiation causes various radiation damages to target materials such as sputtering, defect formation, and plastic deformation. Up to the present considerable efforts have been devoted to understanding of fundamental mechanisms relevant to irradiation effects in a variety of solid materials involving metals, semiconductors and insulators.^{3,4} In most experimental studies, structure and physical properties of materials before and after ion irradiation are measured and examined within a framework of projectile energy loss consideration. This is because the energy loss of projectile ions is a leading key-parameter characterizing radiation effects. It is generally accepted that the energy deposition into a target, via nuclear (recoiling of atoms) and electronic (excitation and ionization) processes, transforms eventually to lattice vibration (heat) and radiation effects are induced during this energy-transforming process. Thus, actual situations relevant to energy transfer and its relaxation are complicated dynamical processes both in time and space. It is, therefore, worth performing *in situ*, or real-time, observation of materials properties to achieve more complete understanding of radiation effects.

Recently we found a new radiation phenomenon for metallic Al foils, exhibiting a large bell-shaped deformation during irradiation of 8 MeV Si^{4+} ions.⁵ The deformation is localized within a beam spot area and is reversible just like a metal spring under beam-on and beam-off conditions. In addition, deformation occurs also in the opposite direction to the incident beam. It implies evidently that the driving force of deformation is not a beam force (momentum transfer) exerted on a target foil. Actually, the beam force is found to be negligibly small and does not play a role as shown in our previous experiments using a torsion balance method.^{6,7}

The purpose of this work is to elucidate the nature of the deformation and to specify the driving force responsible for

the deformation. We used three different types of Al foils and various projectile ions from H to Si of MeV energies. Foil temperatures under ion irradiation were measured as a function of the incident beam flux. Microstructure of foils before and after irradiation was also investigated with a transmission electron microscope. Furthermore, a time-response spectrum of the deformation was measured using a pulsed ion beams, allowing us to obtain rising- and falling-times of the deformation. Present results are examined in terms of the ion-induced thermal energy relaxation model.

II. EXPERIMENTAL

The irradiation experiment was performed with a 1.7 MV Pelletron accelerator at Nara Women's University. The apparatus and experimental procedures were essentially the same as those described in Ref. 5. Three types of polycrystalline Al foils of 2 μm in thickness were used; (type A) an evaporated foil of 99.99% purity (Lebow Co., Ltd., US), (type B) a rolled foil of 99.99% purity (Rikazai Co., Ltd., Japan), and (type C) a rolled foil of 99.7% purity (New Met Koch Co., Ltd., UK). Figure 1 shows a foil-holder in which a foil was sandwiched by two stainless steel plates with a hole of 9 mm in diameter. Any wrinkles or flexures in a foil were removed by carefully pressing a stainless steel guide pipe over the foil surface. An inside open-diameter of the pipe, or the diameter of freestanding area of the foil, was 7 mm. The holder was fixed to a target frame. The projectile ions used were 1 MeV H^+ , 2 MeV C^{2+} , 6 MeV C^{3+} , 3 MeV O^{2+} , 4 MeV O^{3+} , 6 MeV O^{3+} , 3 MeV Si^{3+} , 4 MeV Si^{3+} , 6 MeV Si^{4+} , and 8 MeV Si^{4+} . Care was taken to achieve a uniform beam-intensity distribution. A well-collimated ion-beam of 3 mm in diameter was directed perpendicular to the foil surface at a beam flux ranging from 10^{10} to 10^{12} ions/($\text{cm}^2 \text{ s}$) with a fluctuation less than 10%. The target foil was irradiated at room temperature (28°C) in vacuum below 10^{-5} Pa.

Listed in Table I are irradiation conditions of projectile ions and their energy deposition estimated from the TRIM

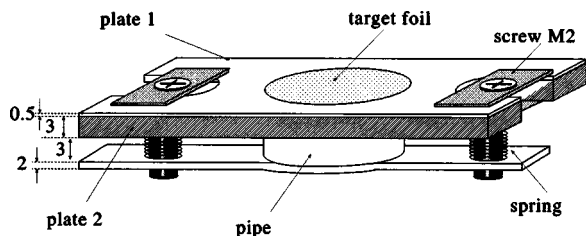


FIG. 1. A schematic sketch of the sample holder.

code.⁸ Projected ranges of all projectile ions are longer than the foil thickness, so that they penetrate completely through the target foil. At the present incident energies, about 95% of the calculated total energy deposition is due to electronic energy loss for all projectiles.

In situ measurements of foil deformation during ion-irradiation were achieved with a laser displacement meter (LDM, model LE-4000 of Keyence, Inc., Japan). The LDM allows us to determine the position of an object with an accuracy of $0.1 \mu\text{m}$ and with a time resolution from 0.5 ms to 1 s. An overall accuracy of the position measurement was about a few μm , arising mainly from mechanical vibration of the experimental chamber. The amount of foil deformation was determined by the difference of positions of the same spot measured for beam-on and beam-off conditions. The LDM was mounted on an X-Y scanning stage driven by a computer-controlled pulse motor. A three-dimensional profile of deformation was obtained by scanning a probe laser beam from the LDM over the backside of the foil. Overall experimental errors through position measurements, including an error due to a fluctuation of beam flux, were about $\pm 10\% - 20\%$.

Time-response behavior of the reversible deformation was measured using a pulsed ion beam obtained by chopping mechanically an incident dc-beam with a double-slit on a rotating drum controlled by a pulse motor. The time-response spectra were obtained by setting the probe laser beam at a peak position of the deformation. The data was taken at 0.5 ms intervals.

Foil temperatures during irradiation were measured with an alumel-chromel thermocouple of 0.1 mm in diameter, which was set in contact with the foil surface. To avoid the thermocouple from beam hitting, measurements were made slightly outside the beam spot boundary.

X-ray diffraction analysis was performed before and after ion irradiation. Also, TEM (transmission electron micros-

copy) observations were carried out to examine microscopic structure of foils for virgin and irradiated areas. The observations were made using a Hitachi H-3000 ultrahigh voltage TEM (UHVEM) at Osaka University operated at 2 or 3 MV.

III. RESULTS

A. TEM observation

Figure 2 shows a typical example of deformation, observed for the foil-A, caused by irradiation of an 8 MeV Si^{4+} beam at a flux of 1.55×10^{12} ions/($\text{cm}^2 \text{s}$). One can see that the deformation profile is bell-shaped, the peak height reaches about $600 \mu\text{m}$, and the deformation rises sharply at a beam spot boundary and appears only within the irradiated area. It is noted that the diameter of the deformed area was about 4 mm, which is 1 mm wider than the beam spot diameter.

Figure 3 shows TEM micrographs of the foil-A for (a) an irradiated area, (b) an unirradiated area (outside of the beam spot), and (c) a boundary area between them, as depicted. The total fluence of incident ions was about 10^{14} ions/ cm^2 . Grain size distributions of these areas, shown in the inset graphs, are found to reveal no significant difference among them and have an average grain size of about 250 nm for all the three areas. This finding suggests that recrystallization does not occur in the irradiated area, or in other words, the temperature of the irradiated area is lower than the recrystallization temperature. The recrystallization temperature was measured by a separate, *in situ*, TEM experiment, where the foil was heated up to 300°C by 50°C increments, and was found to be about 200°C . It implies that the temperature of the ion-irradiated area is below 200°C . Also, x-ray diffraction analysis of the target foils before and after irradiation showed that the lattice constant remained unchanged, indicating that the deformation leaves no strain. TEM micrographs of irradiated areas in the foils of types B and C are shown in Fig. 4, as well as for the foil-A. The average values of the grain size of the foils-B and C were about 2800 and 2880 nm, respectively. Their grain size distributions remained unchanged before and after ion irradiation, as well as for the foil-A.

B. Magnitude of the deformation

We define the magnitude of deformation h as the peak height of bell-shaped deformation (Fig. 2). Experimental re-

TABLE I. Irradiation parameters. E_e and E_n are the electronic and the nuclear energy deposition in Al of $2 \mu\text{m}$ thickness, respectively.

Ion species	H		C		O		Si			
Energy (MeV)	1.00	2.00	6.00	3.00	4.00	6.00	3.00	4.00	6.00	8.00
Projected range ^a (μm)	14.3	2.29	5.40	2.58	3.17	4.29	2.36	2.79	3.54	4.22
E_e^b (MeV)	0.95	1.85	2.54	2.62	3.06	3.45	2.50	3.20	4.30	5.07
E_n^b (keV)	0.043	28.9	5.02	36.9	22.1	12.4	179	121	72.7	50.6

^aData from SRIM 2000.

^bData calculated from the TRIM program.

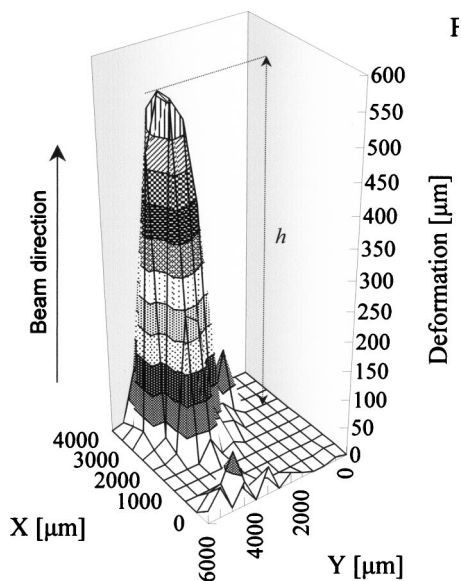


FIG. 2. Three-dimensional deformation profile of foil-A under irradiation of 8 MeV Si^{4+} at a flux of 1.55×10^{12} ions/($\text{cm}^2 \text{ s}$). The positive direction of z -axis corresponds to the direction of the incident beam.

sults of h for three types of foils are shown in Fig. 5 as a function of the incident beam flux of 8 MeV Si^{4+} ions. For all foils, h increases linearly up to a certain value of flux, then increases nonlinearly and becomes constant at high flux region. It is seen that the deformation of the foil-A is considerably larger than those of the foils-B and C, while those of the foils-B and C are nearly the same for each other.

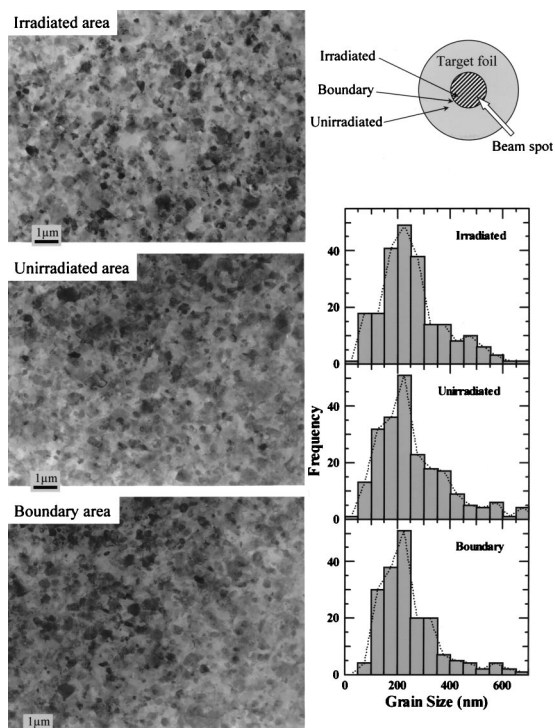


FIG. 3. TEM micrographs of foil-A after ion irradiation obtained for the areas shown in an inset. The grain size distributions are shown by histograms.

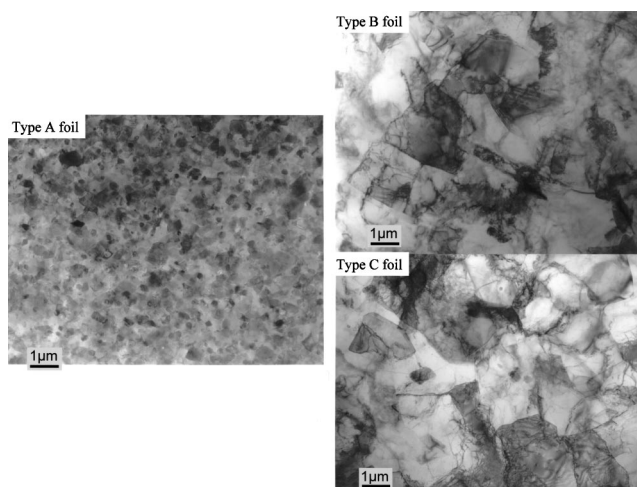


FIG. 4. TEM micrographs of foils-A, B, and C.

A relationship between h and the total energy deposition per projectile into the foil, $E_d (= E_e + E_n)$, was investigated for various combinations of projectile species and incident energies to achieve a wide range of E_d (0.1–5 MeV) as listed in Table I. Here, E_e and E_n are electronic and nuclear energy depositions, respectively. For this measurement a constant beam flux of 2.5×10^{11} ions/($\text{cm}^2 \text{ s}$) was used. Results for the foil-C are depicted in Fig. 6 as a function of E_d , showing a linear relation as shown by a straight line. Since the predominant component of E_d is electronic (Table I), it is evident that the driving force responsible for the deformation is the electronic energy deposition.

C. Foil temperature during ion irradiation

Foil temperatures measured during ion irradiation are shown in Fig. 7 as a function of the beam flux. The measure-

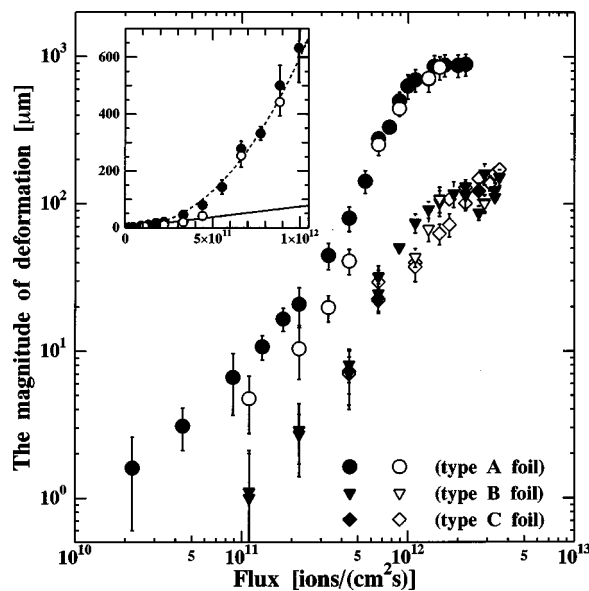


FIG. 5. Flux dependence of the magnitude of foil-deformation during irradiation of 8 MeV Si^{4+} ions. Closed and open symbols represent forward and backward deformations (see text), respectively.

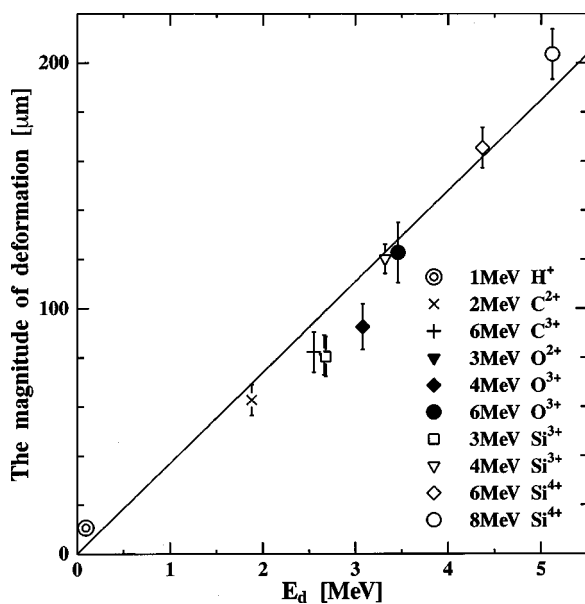


FIG. 6. Magnitude of deformation of foil-C as a function of the total energy deposited into the foil per ion at a fixed flux of 2.5×10^{11} ions/($\text{cm}^2 \text{s}$). A straight line is drawn as a visual aid.

ments were carried out slightly outside a beam spot. The figure shows that the temperatures are nearly proportional to the flux with different slopes depending on the target species and are below the recrystallization temperature of 200°C in the flux range studied. The second result is consistent with the results obtained by TEM observations as described beforehand.

Using a theoretical model^{9,10} developed for the estimation of temperatures of a TEM foil sample under electron irradiation, the temperature rise in a foil under ion irradiation was calculated. In this model it is assumed that a foil is bound by

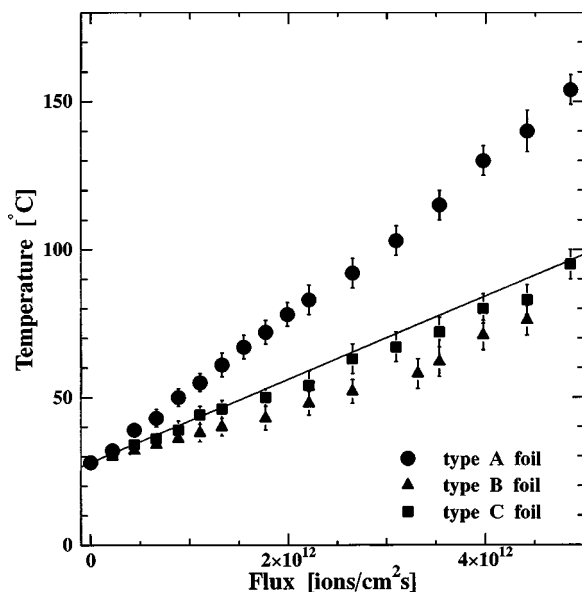


FIG. 7. Foil temperatures measured at a beam spot boundary as a function of the beam flux of 8 MeV Si^{4+} ions. A line is the calculation from Eq. (2).

a circular conductor of infinite conductivity, like our guide pipe, held at a fixed temperature T_0 and the beam intensity is symmetric with respect to the center axis of the conductor. Also, the rate of heat generation per unit volume $H(r)$ is assumed to be independent of the depth of penetration of the incident beam, and is thus solely a function of the distance r from the beam axis. These assumptions are suitable for the present experimental conditions. The temperature $T(r)$ may be calculated by solving the heat conduction equation:

$$\frac{1}{r} \frac{d}{dr} \left(r \frac{dT}{dr} \right) + \frac{1}{\lambda} H(r) = \frac{2\sigma}{\lambda d} (T^4 - T_0^4), \quad (1)$$

where λ the thermal conductivity of a foil, σ the Stefan's constant, and d the thickness of the foil. For metal foils a contribution from thermal radiation is small, so that the temperature is then given by

$$T(r) = T_0 + \frac{H_0 a^2}{4\lambda} \left[Ei \left\{ - \left(\frac{r}{a} \right)^2 \right\} - Ei \left\{ - \left(\frac{b}{a} \right)^2 \right\} + \ln \left(\frac{b}{r} \right)^2 \right], \quad (2)$$

where Ei is the exponential integral function, $a=1.5 \text{ mm}$ and $b=3.5 \text{ mm}$ are the radii of the incident beam and the free-standing area of the foil, respectively, and H_0 is the heat flux expressed by

$$H_0 = I \cdot E_e / d, \quad (3)$$

with I the beam flux and d the foil thickness. Calculated results at the position of the thermocouple ($r=1.5 \text{ mm}$) are shown by a solid line in Fig. 7. Here, we took $\lambda = 240 \text{ W}/(\text{m}\cdot\text{K})$.¹¹ The temperatures at the center of the beam spot ($r=0 \text{ mm}$) were calculated to be about $20\text{--}30^\circ\text{C}$ higher than those at $r=1.5 \text{ mm}$. One can see that the calculated values are in fairly good agreement with experimental results for the foils-B and C, but are substantially smaller than those of the foil-A. It is noted that the foil-A was made by evaporation whereas the foils-B and C were made by cold rolling, so that the density of the foil-A may be different from other foils. Therefore, the fundamental thermophysical properties such as the thermal conductivity are possibly different. It is plausible to state that the value of λ of the foil of type A may be different from that used in the calculation. Assuming the experimental temperatures of the foil-A to be expressed also by Eq. (2), λ is estimated to be about $130 \text{ W}/(\text{m}\cdot\text{K})$. As a conclusion, the difference in results for foil temperatures is closely connected with the density of the foils.

D. Time evolution of the deformation

Time-response spectra of the deformation were measured using pulsed ion beams. By changing the chopping speed of the rotating drum, the rising time (T_B) of the pulsed beam intensity was varied in a range from 5 to 150 ms. Typical examples are shown in Fig. 8 obtained for the foil-A irradiated by 8 MeV Si^{4+} ions. Here, T_B is defined as the time interval between zero and the maximum beam intensity as shown by dotted lines. The foil deformation starts to rise with a certain rise time and drops down according to the

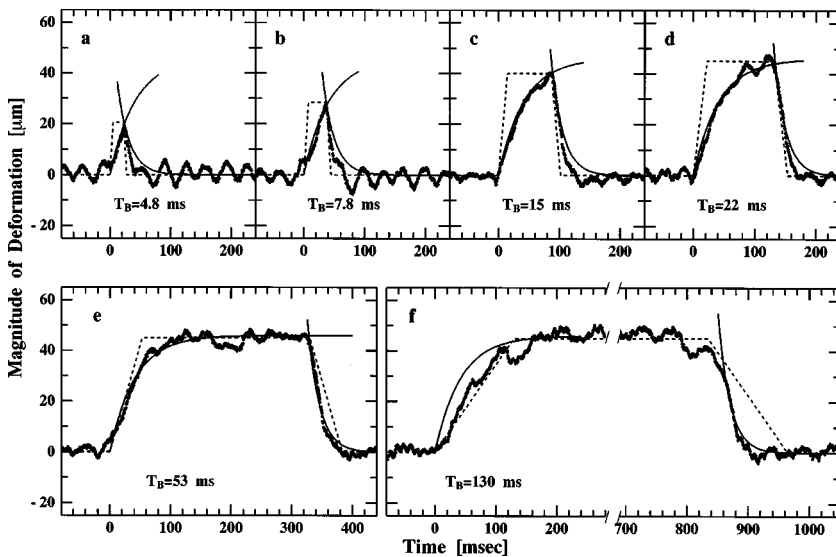


FIG. 8. Time evolution of deformation of foil-A measured for 8 MeV Si⁴⁺ irradiation with six different rise times of pulsed ion beam. Dotted lines denote the beam intensity estimated from the chopper rotation speed, and solid lines are the calculated time profiles.

trapezoidal intensity variation of the incident pulsed beam. The rising parts in the time spectra were found to have almost the same shape irrespective of T_B when T_B is shorter than about 60 ms. For longer T_B (>60 ms), the rising part appears to follow a trapezoidal shape equivalent to the beam intensity [see Fig. 8(f)]. As for the falling part, the profile was found to be essentially the same for all T_B investigated. To demonstrate these characteristics more clearly, two exponential-type functions are drawn by solid lines corresponding respectively to the rising part and the falling part. The time constants used here are 41.6 ms (rising part,) and 19.4 ms (falling part). Time-response spectra were also measured using different ions of 3 MeV Si³⁺ ions for the foils-A and C. Results relevant to the rising- and falling times were essentially the same as those described above. These experimental findings seem to indicate that the time constant is independent of the incident beam energy and the type of foils. Further measurements will be needed to investigate a time-response spectrum of deformation in more detail. As a phenomenological conclusion, it can be stated that the time constant of deformation is of the order of a few tens of ms and the rising time is about twice as large as the falling time.

IV. DISCUSSION

We examine at first the thermal effects with regard to the relative length expansion (RLE) $\Delta L/L$. The RLE may be estimated easily from available standard data¹² once the foil temperature is known. It is important to point out that the RLE data in Ref. 12 increases linearly as a function of the temperature in the range 25–300°C. Using our experimental temperatures $T_{\text{exp}}(I)$ (Fig. 7) and the data in Ref. 12, the RLE were calculated as a function of the beam flux I . Results are shown in Fig. 9 by shaded lines, where upper lines correspond to the center of the beam spot estimated from theoretical temperatures given by Eq. (2).

We also estimated the values of RLE from the peak height data (h) shown in Fig. 5 with assumptions of conical shape for the deformation and three-dimensional isotropic expansion.

The volume of the deformed area during irradiation may be expressed by

$$(1 + \Delta L/L)^3 \pi r_0^2 d = (1 + \Delta L/L) \pi r_0 d \sqrt{r_0^2 + h^2}, \quad (4)$$

where $r_0=2$ mm is the cone radius of the deformed area (see Fig. 2). Estimated values of $\Delta L/L$ are shown in Fig. 9. Note that to these estimated values of $\Delta L/L$, a value of $\Delta L/L$ at room temperature (28°C) derived from the data in Ref. 12 is added, since Eq. (4) gives a relative length expansion asso-

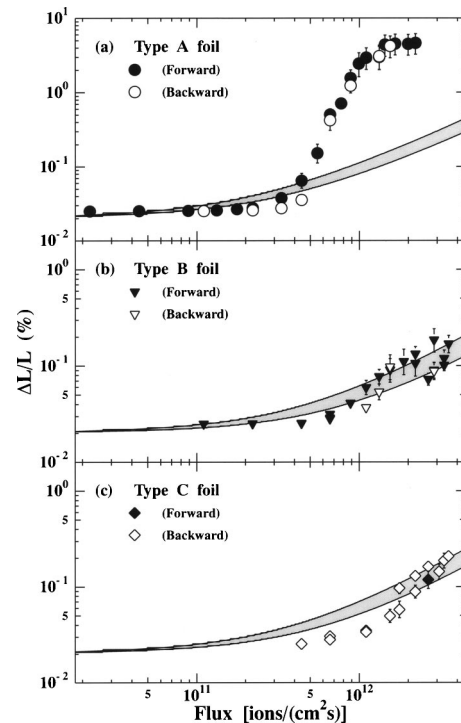


FIG. 9. Relative length expansion $\Delta L/L$ as a function of the beam flux. Shaded lines show the theoretical estimations obtained using the thermal linear expansion data (Ref. 12) and temperatures shown in Fig. 7. The direction of foil deformation is denoted by “Forward” and “Backward.”

ciated with ion irradiation effects ($\Delta L/L=0$ for $h=0$, corresponding to no beam flux). Estimated values for the foils-B and C are in fairly good agreement with those from the standard data,¹² while again for the foil-A, significant discrepancies occur in a higher beam flux region. This discrepancy may be due to the fact that the foil-A, made by evaporation, has lower thermal conductivity. Foil-temperature measurements, shown in Fig. 7, indicate that the foil-A may be heated to relatively higher temperatures than other foils. Hence, the enhancement of RLE of the foil-A is attributed to the anomalous beam heating due to poor thermal conductivity. We expect that such anomalous heating effects result in a significantly large expansion of lattice constant and the creation of many vacancies, leading to an additional volume expansion besides the thermal expansion.

Next, the thermal effects are examined with regard to the characteristic time response of the deformation. By solving a time-dependent equation for the heat conduction,¹³ the time constant of temperature variation may be obtained as,

$$\tau = \frac{\pi a^2 d \rho c (T_1 - T_0)}{H_0 d}, \quad (5)$$

where, T_0 the room temperature, T_1 the equilibrium temperature during ion irradiation, ρ and c are the density and the specific heat of the foil, respectively. In the present work, the actual values of ρ and c were not known, so that rough estimation of τ was made. Using standard values of $\rho = 2.7 \text{ g/cm}^3$ and $c = 2.4 \text{ J/(g}\cdot\text{K)}$ for Al materials, the values of τ estimated from the slopes of Fig. 7 are 40, 16, and 21 ms for foils-A, B, and C, respectively.

The estimated results mean that the time constant of thermalization is of the order of a few tens of ms and it depends on the foil species. We find, therefore, that the time constants of thermalization are the same order as the foil deformation. If the foil deformation is caused by thermal effects, the time evolution should follow the time constant of thermalization. In this case, the time response profile of deformation should be symmetric because heating and cooling time of a foil is expected to be the same as given by Eq. (5). However, observed time-response profile of deformation, shown in Fig. 8, is asymmetric. It should be emphasized that the foil deformation occurs only during ion irradiation. Namely, constitu-

ent atoms of a foil during irradiation-induced deformation may be in a quasi-steady phase of ionization and excitation due to ion-solid interactions. Consequently, the amount of heat flow which affects the thermalization may be different for irradiation and nonirradiation conditions, giving rise to different time constants of deformation during irradiation (rising time) and nonirradiation (falling time). To understand the foil deformation more accurately, it is necessary to take account of dynamical thermophysical properties of materials during ion irradiation.

V. SUMMARY

We have investigated the fundamental nature of reversible deformation of metallic Al foils during MeV energy ion beam irradiation. It was found that the electronic energy deposition is the dominant driving force of the deformation. The magnitude of deformation was found to depend on the foil species. A significantly large deformation was observed for the foil made by evaporation and was found to occur at foil temperatures below the recrystallization temperature of 200°C. In this case, a large expansion of lattice constant or creation of many vacancies are expected during foil deformation. In order to understand the mechanism in more detail, it is necessary to perform further in situ experiments on the lattice constant and the lattice-vacancy creation during foil deformation by using various incident beams of ions, electrons and photons (laser).

ACKNOWLEDGMENTS

We would like to thank Dr. N. Kishimoto at NIMS, Dr. M. Kiritani, Dr. M. Komatsu at Hiroshima Inst. Tech., Dr. N. Yamada at AIST, Dr. H. Nakajima at Osaka University, and Dr. H. Matsui at Tohoku Univ. for their useful comments and valuable suggestions. We also thank J. Karimata, M. Kobayashi, and S. Kamakura for their experimental assistance, and Dr. K. Yamamoto for his technical support during x-ray diffraction experiments. Authors (I.K. and S.C.J.) acknowledge the encouragement from Dr. T. Nomura and the E-group staff of KEK. This work was supported by a Grant-in-Aid from the Ministry of Education, Culture, Sports, Science, and Technology (MEXT), Japan, and partly by “Nanotechnology Support Project” of the MEXT.

*Present address: Quantum Science and Engineering Center, Kyoto University, Kyoto 606-8501, Japan. Electronic mail address: tsuchida@nucleng.kyoto-u.ac.jp

¹M. Nastasi, J. W. Mayer, and J. K. Hirvonen, *Ion-Solid Interactions: Fundamentals and Applications*, edited by D. R. Clarke, S. Suresh, and I. M. Ward FRS (Cambridge University Press, Cambridge, U.K., 1996).

²H. Schmidt-Böcking, A. Schempp, and K. E. Stiebing, *Materials Research with Ion Beams* (Springer-Verlag, Berlin, 1992).

³J. C. Slater, *J. Appl. Phys.* **22**, 237 (1951).

⁴For instance, as a recent conference proceedings, *Proceedings of Fifth International Symposium of Swift Heavy Ions in Matter*, Nucl. Instrum. Methods Phys. Res. B **209** (2003).

⁵H. Tsuchida, I. Katayama, S. C. Jeong, H. Ogawa, N. Sakamoto, and A. Itoh, *AIP Conf. Proc.* **576**, 931 (2001).

⁶H. Tsuchida, I. Katayama, S. C. Jeong, H. Ogawa, N. Sakamoto, and A. Itoh, *Trans. Mater. Res. Soc. Jpn.* **28**[2], 413 (2003).

⁷I. Katayama, S. C. Jeong, H. Tsuchida, H. Ogawa, N. Sakamoto, and A. Itoh, *J. Chin. Chem. Soc. (Taipei)* **48**, 455 (2001).

⁸J. Ziegler, J. F. Biersack, and U. Littmark, *The Stopping and Range of Ions in Matter* (Computer Code SRIM Version 2000)

(Pergamon Press, New York, 1985).

⁹B. Gale and K. F. Hale, *Br. J. Appl. Phys.* **12**, 115 (1961).

¹⁰S. B. Fisher, *Radiat. Eff.* **5**, 239 (1970).

¹¹G. K. White, in *Metals: Electronic Transport Phenomena*, edited by K.-H. Hellwege and O. Madelung, Landolt-Börnstein, New Series, Group III, Vol. 15, Part C (Springer-Verlag, Berlin,

1991), p. 12.

¹²Y. S. Touloukian, R. K. Kirby, R. E. Talor, and P. D. Desai, *Thermophysical Properties of Matter, The TPRC Data Series*, Vol. 12 (IFI/Plenum, New York-Washington, 1975).

¹³H. S. Carslaw and J. C. Jaeger, *Conduction of Heat in Solids*, 2nd ed. (Clarendon Press, Oxford, 1959).